Organizing Principles for a Diversity of GABAergic Interneurons and Synapses in the Neocortex

Anirudh Gupta *et al.*

Science **287**, 273 (2000);
DOI: 10.1126/science.287.5451.273

Organizing Principles for a Diversity of GABAergic Interneurons and Synapses in the Neocortex

Anirudh Gupta,* Yun Wang,* Henry Markram†‡

A puzzling feature of the neocortex is the rich array of inhibitory interneurons. Multiple neuron recordings revealed numerous electrophysiological-anatomical subclasses of neocortical γ-aminobutyric acid–ergic (GABAergic) interneurons and three types of GABAergic synapses. The type of synapse used by each interneuron to influence its neighbors follows three functional organizing principles. These principles suggest that inhibitory synapses could shape the impact of different interneurons according to their specific spatiotemporal patterns of activity and that GABAergic interneuron and synapse diversity may enable combinatorial inhibitory effects in the neocortex.

The difficulty in understanding the organization and function of the GABAergic system is due to the large diversity of anatomically and physiologically distinct neurons (*1*–*4*). GABAergic synaptic transmission in the neocortex has mostly been studied with extracellular electrical stimulation and in some cases by obtaining paired recordings (*2*, *5*, *6*). We recorded from a large number of interneuron connections and explored whether the nature of the synaptic outflow from interneurons could reveal the way in which the GABAergic system is organized and functions. Multiple whole-cell patch-clamp recordings were used to characterize key properties of synapses formed by anatomically and physiologically distinct interneurons: (i) the kinetics of GABAergic receptors used at synapses, (ii) the number and precise locations of putative synapses forming a connection, (iii) the absolute strength of connections, and (iv) the particular temporal dynamics of synaptic transmission that arise because of an interaction between the rate of neurotransmitter release [depending on probability of release (*P*) and the frequency of stimulation], the rate of recovery from release (synaptic depression), and the rate of recovery from facilitation of release (*7*, *8*). Temporal dynamics of synapses may be particularly important because this could determine the temporal impact on target neurons.

Diversity of GABAergic Synapses

Infrared differential interference contrast microscopy was used to visually select neurons for recording within layers II to IV of somatosensory cortex in neocortical slices of Wistar rats (postnatal day 13 to 16) (*9*). Potential presynaptic interneurons were distinguished from postsynaptic pyramidal neurons according to their bipolar or multipolar dendritic appearance as well as their oval or round somata. Neurons were recorded simultaneously with the whole-cell patch-clamp technique (*9*), and interneuron identity was confirmed by the repertoire of electrophysiological responses to current injections. About 800 quadruple recordings were obtained, yielding around 3000 potential GABAergic connections. There were more than 240 GABAergic connections, of which 179 were studied in detail (*10*). The GABAergic nature of the connections was routinely verified by determining the reversal potential of the synaptic response (*11*) and, in some cases, also by applying the GABA-A receptor antagonist, bicuculline. Neurons were filled with biocytin to allow staining and anatomical three-dimensional (3D) computer reconstructions of the physiologically characterized connections (*9*, *12*, *13*).

Synaptic connections were examined by eliciting short trains of precisely timed action potentials (APs) in interneurons across a range of physiologically relevant discharge frequencies (5 to 70 Hz), followed by a recovery test response (RTR) 500 ms later. The inhibitory postsynaptic potentials (IPSPs) or the currents (IPSCs), or both, were recorded (*14*). The average synaptic response to this stimulation protocol allows the extraction of the basic parameters of the synaptic connection with a model of dynamic synaptic transmission (*9*) (*U*, equivalent to average *P*; *F*, the time constant to recover from facilitation; *D*, the time constant to recover from depression; *A*, the absolute strength of the connection, which is equivalent to the product of quantal size and number of release sites) as well as the statistics of the transmission [coefficient of variation (CV) and failures of transmission].

GABAergic synaptic responses were highly

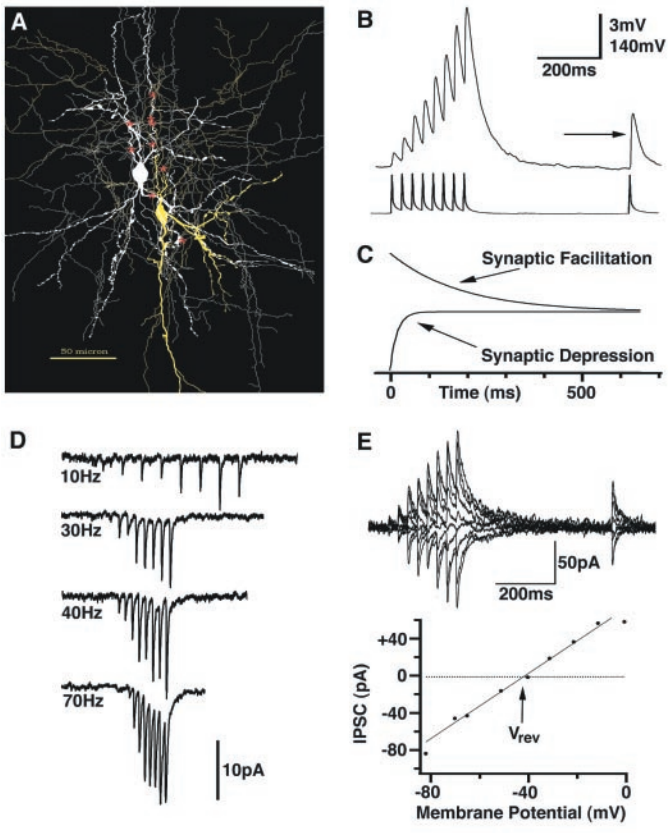

Fig. 1. F1 GABAergic synaptic connections. (**A**) 3D computer reconstruction of connected interneurons (IN). Red stars, putative synapses (*9*, *12*) formed by presynaptic (yellow) BTC (*21*) onto postsynaptic (white) SBC (*19*). (**B**) Average IPSPs [trials (t) = 30] recorded in SBC [upper trace, holding potential (V_{HOLD}), −75mV] to stimulation of BTC (lower AP trace). Arrow, RTR. (**C**) Schematic representation of synaptic facilitation outlasting depression (arbitrary scales). (**D**) Average IPSCs (t = 30) to different stimulation frequencies. (**E**) Average IPSCs (t = 5) at different potentials (V_{HOLD}, −80 to 0 mV) (*28*). Arrow, reversal potential (V_{rev}). Lower graph: RTR amplitudes versus V_{HOLD} (dots) (line fit, regression coefficient 0.98; V_{rev}, −40.6 mV).

Department of Neurobiology, The Weizmann Institute for Science, 76100 Rehovot, Israel.

*These authors contributed equally to this work.
†Present address: Keck Center for Integrative Neurosciences, 828-HSE, University of California at San Francisco, San Francisco, CA 94143–0732, USA.
‡To whom correspondence should be addressed. E-mail: Henry.Markram@weizmann.ac.il

Table 1. Summary of GABAergic synaptic properties in neocortical layers II to IV. Occurrence: Synaptic classification is according to facilitated (F1, >10%), depressed (F2, >10%), and recovered (F3) RTR. This classification is verified for 65/65 cases. Synaptic model parameters: Model fit of connections with too few trials, test frequencies, small responses, or high CVs produced high-fit errors (*29*). For F2, modeling was performed on a random subset because of large data volume. Analysis of variance (ANOVA) on log-transformed raw data (*F:D* ratios), $F = 274$, with (2,62) df, $P = 0.0001$. Fisher's multiple comparison (at $\alpha = 0.05$) showed that the groups differ significantly from each other (all three pairwise, $P < 0.01$). Synaptic release statistics: Failure and CV analyses were carried out only in connections with more than 50 trials. Failures are defined as events with amplitudes smaller than 1.59 pA or 60 μV. CV (SD/mean of 80 to 150 traces) values were overestimated by 2.74 ± 1.97% in VC ($n = 13$) and by 0.78 ± 0.77% in CC ($n = 13$). Failure rate and CV of F1 connections are significantly different from those of F2 and F3 ($P < 0.01$). Student's *t* tests were performed to determine statistical differences. Decay time constant (DTC) of IPSCs was estimated as single exponentials, because of multiple distributed release sites. Chord conductance (G_1) was determined as slope of line fit through amplitudes of first responses and intersection at the reversal potential (negligible rectification detected). $G_{max} = G_1/U$. Per synapse conductance (G_{syn}) = G_{max}/anatomically estimated number of synapses or binomially calculated number. G_{max} for F2 connections was significantly different from that for F1 and F3 connections ($P < 0.02$). Synaptic numbers and distances: Anatomical *n* was estimated as in (*12*). Binomial $n = 1 - P/CV^2P$, where *P* is the probability of neurotransmitter release and *n* is the binomial number of release sites. *P* was replaced by *U* derived from the model of nonlinear synaptic transmission. Steady-state electrotonic distances computed according to (*7*). All values shown above are mean ± SD, except for *F:D* and *D:F* ratios, which are mean ± SEM.

	F1 GABAergic synapses	F2 GABAergic synapses	F3 GABAergic synapses
		Occurrence	
Total	24/179 (13.4%)	128/179 (71.5%)	27/179 (15.1%)
IN to PC	10/131 (7.6%)	100/131 (76.3%)	21/131 (16%)
IN to IN	14/48 (29.2%)	28/48 (58.3%)	6/48 (12.5%)
		Synaptic model parameters	
U	0.16 ± 0.1 ($n = 14$)	0.25 ± 0.13 ($n = 38$)	0.32 ± 0.14 ($n = 13$)
F (ms)	376 ± 253 ($n = 14$)	21 ± 9 ($n = 38$)	62 ± 31 ($n = 13$)
D (ms)	45 ± 21 ($n = 14$)	706 ± 405 ($n = 38$)	144 ± 80 ($n = 13$)
F:D ratio	9.04 ± 1.85 ($n = 14$)	—	—
D:F ratio	—	40.1 ± 4.6 ($n = 38$)	2.82 ± 0.46 ($n = 13$)
		Synaptic release statistics	
Failures (%)	26.8 ± 26.3 ($n = 18$)	5.14 ± 8.7 ($n = 90$)	8.89 ± 11.85 ($n = 21$)
CV of first response amplitude	0.91 ± 0.56 ($n = 18$)	0.46 ± 0.17 ($n = 90$)	0.53 ± 0.23 ($n = 21$)
		Synaptic currents and conductances	
DTC of IPSC (ms)	10.41 ± 6.16 ($n = 9$)	8.3 ± 2.2 ($n = 52$)	6.44 ± 1.7 ($n = 4$)
G_{max} (nS)	3.24 ± 2.6 ($n = 8$)	7.76 ± 6.6 ($n = 15$)	3.44 ± 0.84 ($n = 4$)
G_{syn} (nS) based on anatomical *n*	0.35 ± 0.28	0.49 ± 0.41	0.2 ± 0.05
G_{syn} (nS) based on binomial *n*	0.33 ± 0.27	0.32 ± 0.28	0.2 ± 0.05
		Synapse numbers and distance	
Anatomical *n*	9.3 ± 3.1 ($n = 3$)	16 ± 5.5 ($n = 21$)	16.7 ± 11.9 ($n = 7$)
Binomial *n*	9.8 ± 7.2 ($n = 14$)	24 ± 9.9 ($n = 24$)	17 ± 7.7 ($n = 13$)
Steady-state electronic distance	0.085 ± 0.071 (28 synapses)	0.092 ± 0.074 (324 synapses)	0.08 ± 0.067 (116 synapses)

diverse in terms of their temporal dynamics: The RTRs were either facilitated, depressed, or unchanged as compared with the first response in the AP train, suggesting that GABAergic synapses differ in the extent to which they undergo synaptic depression and facilitation. *F* was ~10 times as great as *D* at connections with facilitated RTRs, *D* was ~40 times as great as *F* at connections with depressed RTRs, and *F* and *D* were similar at connections where RTRs were unchanged (Table 1). The *F:D* ratios of these three types of synaptic responses were statistically distinct from each other with no overlap in their distributions. We refer to these three types of responses as F1 to F3, respectively.

Figure 1A shows a reconstruction of an F1 GABAergic connection between two interneurons, and Fig. 1B shows the facilitating synaptic response recorded from this connection. Nine putative synapses were identified (Table 1). F1 connections typically displayed the lowest *U* values, the highest failure rates of all connections, and, accordingly, the highest CVs for the amplitudes of the first response in the train (Table 1). The low *U* values are required for expression of synaptic facilitation. Both synaptic facilitation and depression are engaged during the train, but facilitation persists longer than depression (Fig. 1C), resulting in a facilitated RTR and increased amplitudes of responses as the frequency of the presynaptic APs increases (Fig. 1D). Other parameters, such as the conductance per synapse (G_{syn}) and the kinetics of the synaptic current obtained from voltage-clamp experiments, were not significantly different from those of the F2 and F3 GABAergic connections (Table 1). F1 synaptic connections appeared to be mediated only by GABA-A receptors (Fig. 1E).

F2 GABAergic synaptic connections were the most common type encountered (Fig. 2A). They displayed depression at low frequencies (Fig. 2B, 5-Hz trace), but prominent facilitation

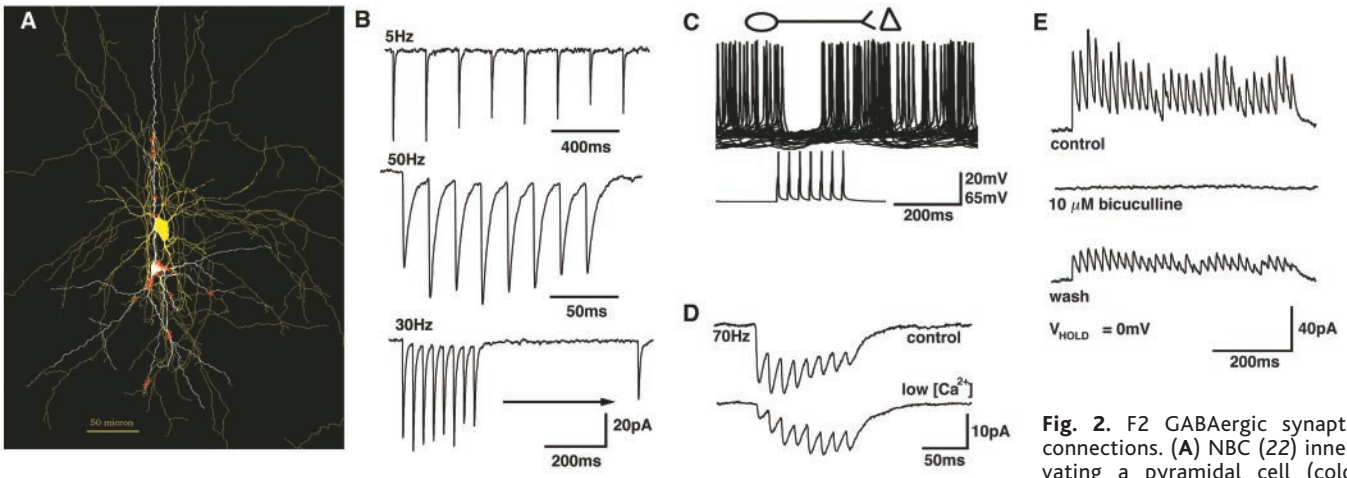

Fig. 2. F2 GABAergic synaptic connections. (**A**) NBC (*22*) innervating a pyramidal cell (color code as in Fig. 1). (**B**) Average IPSCs (t = 30) at different stimulation frequencies. V_{HOLD}, −75 mV. Arrow, RTR. (**C**) Spontaneous AP discharge (30 trials overlaid, ~5 to 10 Hz) of a postsynaptic PC (upper traces) with stimulation of presynaptic IN (lower trace). (**D**) Average IPSCs (t = 40) before (upper trace) and in low $[Ca^{2+}]_{bath}$ (lower trace) (*15*). (**E**) Average IPSCs (t = 30) before, during, and after bath application of 10 μM bicuculline.

at higher frequencies (50-Hz trace). F2 synapses are characterized by depressed RTRs (30-Hz trace). Not only was the RTR depressed compared with the first response but also compared with the last response in the train (30-Hz trace, arrow). Naïvely, it would appear that synapses become more depressed during the recovery period. This behavior, however, is due to brief facilitation of responses during the train, whereas facilitation is absent by the time of the RTR. Because of this brief facilitation and the longer lasting depression, activation of these synapses can effectively, but only transiently, block AP discharge (Fig. 2C). Facilitation was not always observed because U was too high to allow its expression. Nevertheless, the apparently negative, nonexistent, or unrealistically slow recovery from synaptic depression (as estimated from the RTR) predicted that these synapses were F2 type synapses; this was confirmed by lowering extracellular [Ca^{2+}] (*15*), which lowers U ($n = 4$; Fig. 2D).

The number of release sites estimated with a binomial analysis was considerably higher than the number of putative synapses estimated anatomically (Table 1). Despite lower U values, F2 connections also displayed lower CV values than F3 connections. Because most errors in the anatomical (*12*, *13*) and binomial estimates would increase this discrepancy, we propose that F2 synapses use multiple release sites. Indeed, electron microscopic evidence does support multiple release sites at some GABAergic synapses in the neocortex (*13*, *16*). The physiological and anatomical properties of F1 and F3 connections do not suggest that these types of connections use multiple release sites. As for F1 and F3 connections, only GABA-A receptors appear to mediate the transmission (Fig. 2E).

The third type of GABAergic connection (Fig. 3A) not only remained in a facilitated state briefly but also recovered from synaptic depression rapidly. This results in equal amplitude synaptic responses at low frequencies (Fig. 3B; 10-Hz trace). However, at high frequencies, facilitation is revealed if U is sufficiently low to permit the dynamic range required to observe facilitation (Fig. 3B; 70-Hz trace). Regardless of U and frequency, the synapses recover completely by the time of the RTR. F3 connections displayed the highest U values, indicating that these connections reliably produce the largest GABA output during high-frequency stimulation.

Anatomical Diversity of GABAergic Interneurons

Figure 4 shows examples of anatomical reconstructions of five classes of interneurons that innervate pyramidal cells (PCs). Sixty-one of 131 of the most extensively stained neurons were subjected to morphometric analysis (*12*). Typical basket cells (BCs, 12/61, 19.7%) (*17*) were recorded primarily in layer IV. These multipolar cells with aspiny dendrites gave rise to long horizontal axon collaterals. The axon Sholl distance (ASD) (*18*) for BCs was 200.4 ± 31.6 μm (six connections), and the mean axonal segment length (ASL) was 47.2 ± 11.5 μm (*18*). BCs also formed a high fraction (at least 19%) of their putative synapses on somata of target cells. Small basket cells (SBCs, 9/61, 14.8%) (*19*) exhibited characteristic dense local clusters of axon collaterals with only a few far reaching collaterals. The cluster is reflected by a greater number of shorter axon segments (ASL, 32.9 ± 9.0 μm; $n = 7$), a significantly greater bouton density (0.22 ± 0.03 boutons/

Table 2. Summary of GABAergic innervation of PCs. Mapping of GABAergic synapses (F1 to F3) according to presynaptic interneurons defined with anatomical [upper section (*17–22*)], electrophysiological (middle section) (Fig. 5), and a combination of both anatomical and electrophysiological criteria (lower section).

Anatomy	Physiology	Synapse	Number of cases
	Mapping synaptic classes onto neuronal anatomy		
BC		F2	12
SBC		F1	3
		F2	3
		F3	3
NBC		F2	12
		F3	5
MC		F2	11
		F3	2
BTC		F2	10
	Mapping synaptic classes onto neuronal physiology		
	c-AC; b-AC	F1	7; 2
	c-AC; d-AC; b-AC	F2	20; 4; 1
	c-NAC; d-NAC	F2	16; 23
	c-NAC; d-NAC; b-NAC	F3	4; 2; 1
	b-STUT	F1	2
	c-STUT	F2	4
	c-STUT; b-STUT	F3	4; 2
	Mapping synaptic classes onto combined neuronal anatomy and physiology		
BC	c-NAC	F2	6
	d-NAC	F2	3
SBC	c-AC	F1	3
	c-NAC	F3	3
	d-NAC	F2	2
NBC	c-AC	F2	4
	b-STUT	F3	1
	d-NAC	F2	6
	c-NAC	F3	1
MC	c-AC	F2	3
	b-STUT	F3	1
	c-NAC	F2	4
BTC	c-AC	F2	2
	d-NAC	F2	2

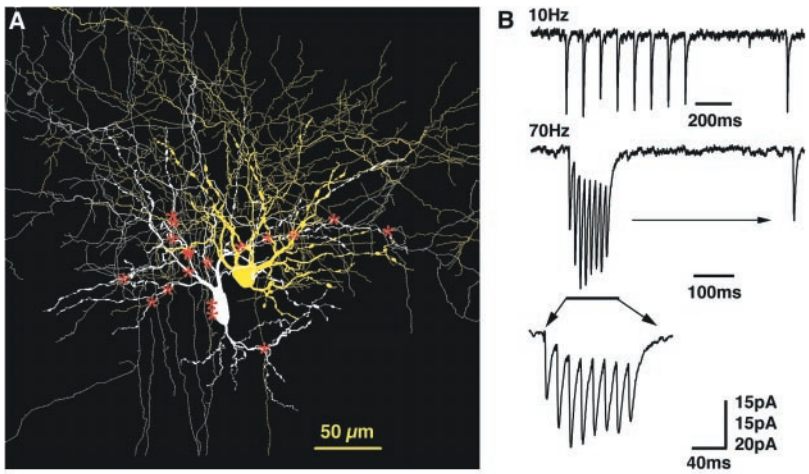

Fig. 3. F3 GABAergic synaptic connections. (**A**) BC (*17*) innervating MC (*20*) (color code as in Fig. 1). (**B**) IPSCs (t = 30) at low and high frequencies. Arrow, RTR. Expanded on time scale, lower trace.

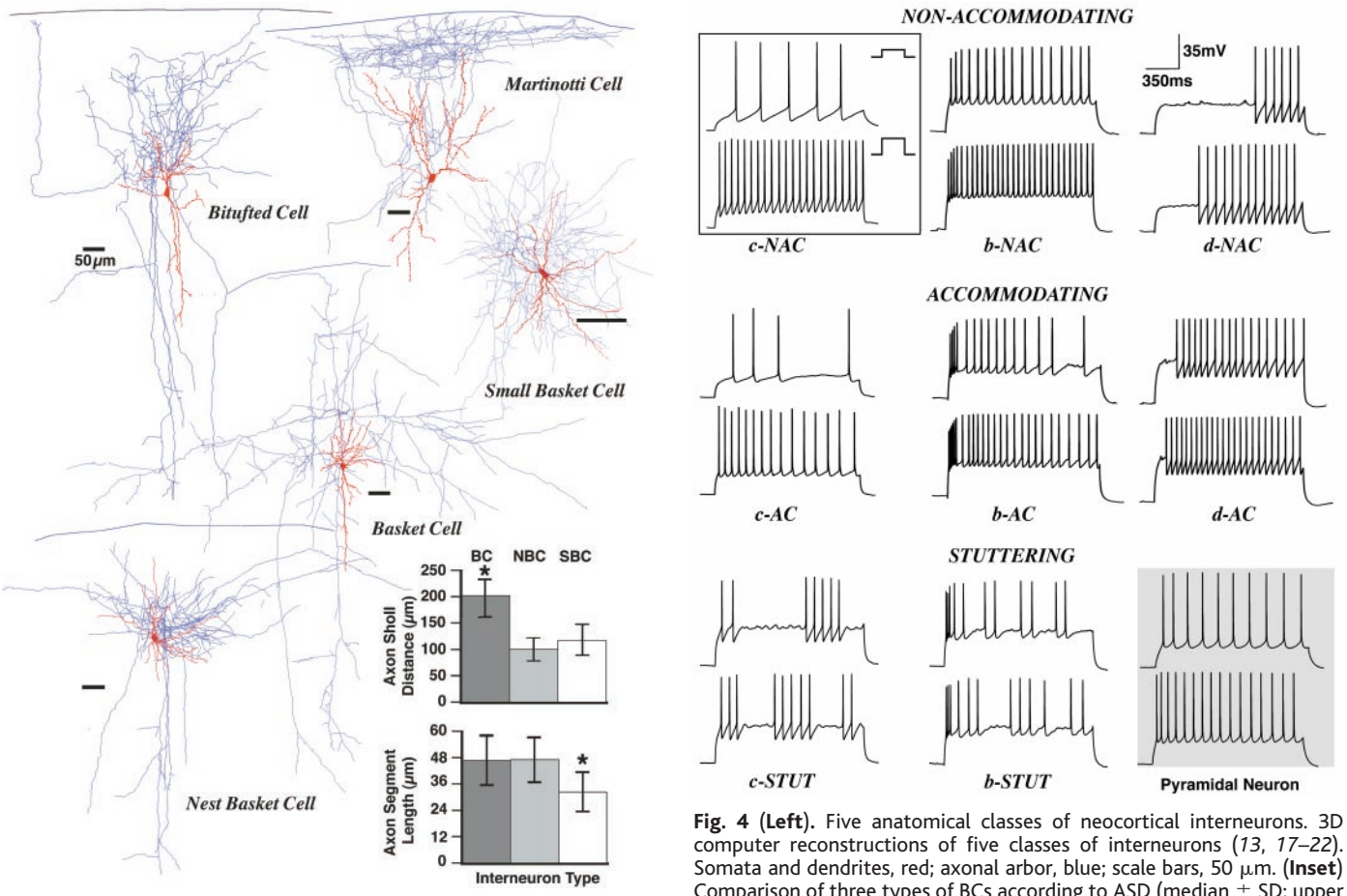

Fig. 4 (Left). Five anatomical classes of neocortical interneurons. 3D computer reconstructions of five classes of interneurons (*13*, *17–22*). Somata and dendrites, red; axonal arbor, blue; scale bars, 50 μm. (**Inset**) Comparison of three types of BCs according to ASD (median ± SD; upper graph) (*18*) and ASL (mean ± SD). *, $P < 0.05$.

Fig. 5 (Right). Three classes and eight subclasses of interneurons. Representative responses to low (30 to −70 pA; upper traces) and high (90 to −160 pA; lower traces) somatic current injections. Classes according to nonaccommodating (NAC, upper six traces), accommodating (AC, middle six traces), and stuttering behavior (STUT, bottom four left traces). Bottom right, "regular spiking" responses from PCs. Subclasses according to classical (c, leftmost traces), burst (b, middle traces), and delayed (d, rightmost traces) discharge. V_{HOLD}, ~−75 mV, for all traces. Discharge properties stable for V_{HOLD} from −85 to −60 mV. Average of five interspike intervals (ISIs) determined for discharge responses evoked by three different amplitudes of current injection beginning from middle of AP train and compared with average of last five ISI. Degree of accommodation: NAC (8 ± 1.9%; $n = 6$); AC (38.4 ± 19.6%; $n = 6$). Stuttering cells display unpredictable short trains of action potentials even during very high current injections.

μm; $P < 0.05$), and lower ASD values than BCs (116.2 ± 29.3 μm; Fig. 4, inset). SBCs also formed some synapses onto somata of both pyramidal cells as well as interneurons (at least 5%). Martinotti cells (MCs,13/61, 21.3%) (*20*) exhibited distinctive axonal arborizations with collaterals reaching layer I and contacting tuft dendrites of PCs (30% of putative synapses). The angle of axonal branches in MCs (80.7 ± 5.1°; $n = 7$) was much wider than in BCs and SBCs (BC, 66.7 ± 6.2°; SBC, 73.1 ± 6.2°). Bitufted cells (BTCs, 10/61, 16.4%) (*21*) gave rise to primary dendrites emerging on opposite poles and exhibited distinct axonal arborization. The wide angled (77.2 ± 4.3°; $n = 7$) and curvy collaterals innervated primarily the dendritic regions of target cells.

A fifth anatomical class of interneuron frequently encountered (17/61; 27.9%; mostly in layers II and III) did not fit the set of properties of typical interneurons previously described [but see (*22*)]. This class of interneuron seems to be a hybrid of SBCs and BCs, because they exhibit a local nest of axons around the somata and long extending axons. Like BCs and SBCs, they form synapses on somata (at least 16%) and exhibit similar axonal branch angles (68.9 ± 5.4°; $n = 7$). They differ from BCs in their ASD (less than half the value, 99.1 ± 21.4 μm) and from SBCs in their ASL (nearly 50% longer, 47.5 ± 10.2 μm) (Fig. 4, inset). We name this interneuron a "nest basket cell" (NBC). NBCs exhibit the richest diversity of electrophysiological subtypes.

Electrophysiological Diversity of GABAergic Interneurons

Although interneurons may display many types of responses in vivo (*23*), under controlled conditions in vitro, differences in biophysical properties manifest in distinct electrophysiological responses. The physiology of pyramidal neurons in layers II to IV was relatively uniform and has previously been described as "regular spiking" (Fig. 5) (*4*). However, for neocortical interneurons, the usual classification of "fast spiking," "bursting," and "regular spiking" (*4*) was too vague to encompass the diversity of responses. The electrophysiological responses presented as three main classes and eight distinct subclasses, many of which have not been reported previously. We began with a broad classification into nonaccommodating (45/91, 49.4%, NAC), accommodating (34/91, 37.4%, AC), and stuttering cells (12/91, 13.2%, STUT) (*24*). These major classes were further subdivided into three subclasses according to (i) the presence of a burst response at the onset of the step depolarization (b-NAC, b-AC, b-STUT), (ii) a delay of variable duration until the onset of AP discharge (d-NAC, d-AC; probably due to the presence of transient outward K^+ currents) (*25*), and (iii) the absence of either a burst or a delay in the response, referred to as a classical response (c-NAC, c-AC, c-STUT). Delayed onset discharge has previously been reported definitively only for neurogliaform interneurons in layers II and III (*24*), but we found this class of response also for several other anatomically distinct interneurons.

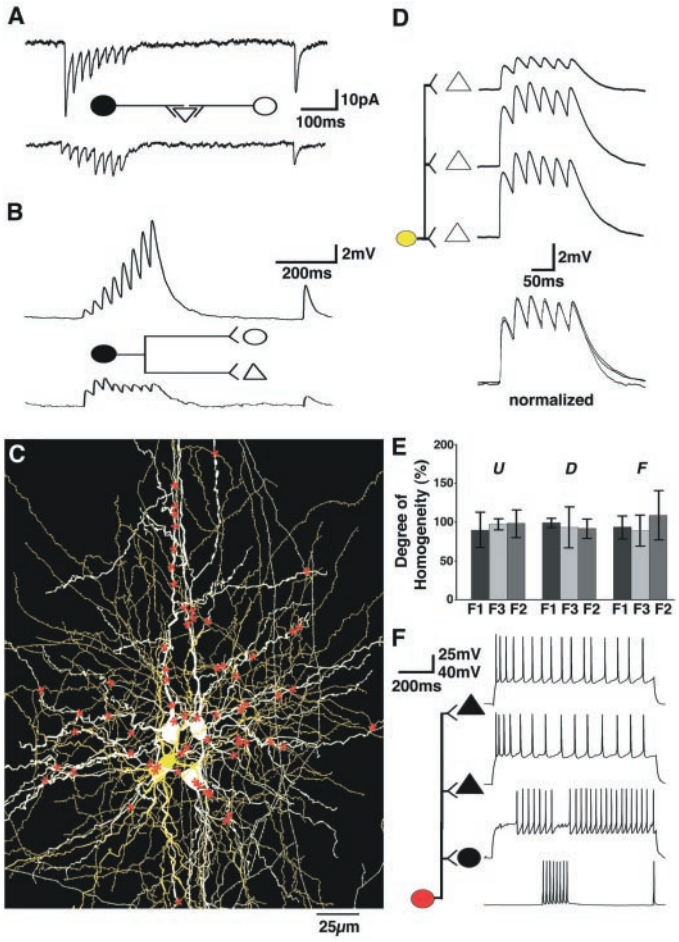

Fig. 6. GABAergic microcircuitry. Simultaneous triple and quadruple neuron recordings. (**A**) Average IPSCs (t = 30) recorded in a PC (triangle) to stimulation of two different INs (circles); V_{HOLD}, −75 mV. (**B**) Average IPSPs (t = 30) recorded in two different postsynaptic neurons to stimulation in a single presynaptic IN. V_{HOLD}, −75 mV. (**C**) SBC (*19*) innervating three PCs (color code as in Fig. 1). (**D**) Average IPSPs (t = 40) recorded in three PCs (upper traces, 30 Hz; V_{HOLD}, −75 mV) to stimulation of SBC [illustrated in (C)]. Traces normalized to first response amplitude (lower traces, overlaid). (**E**) Degree of homogeneity for *U*, *D*, and *F* for 13 divergent connections (one connection randomly taken as control and the percentage of deviation for the others calculated; mean ± SD). (**F**) Presynaptic IN causes delayed spike blocking (because of F1 dynamics) in target IN, but not in target PCs (because of differences in *A*). Input resistances of target cells: 100, 120, and 130 Mohms. Scale bar, 40 mV, lowermost trace.

A Synapse Mapping Principle

After establishing the anatomical and electrophysiological classes of interneurons recorded, we addressed the organizing principles that determine the types of synapses formed by each different class of interneuron onto pyramidal cells. Interneurons defined solely on anatomical or electrophysiological grounds formed different types of synapses (Table 2). However, subclassifying the anatomically defined interneurons according to their electrophysiology revealed 14 distinct subclasses of interneurons and perfect mapping of synapse types (Table 2) (*26*, *27*). These data show that specific interneurons form specific types of synapses on pyramidal cells. The synaptic organization onto interneurons was also examined and some connections defined. As for PCs, we found that different types of synapses formed onto different anatomically or electrophysiologically defined interneurons, suggesting that inter-interneuron synapses probably also obey the same mapping rules.

A Presynaptic-Postsynaptic Interaction Principle

The finding that various classes of interneurons can establish different types of synapses onto the same class of target neuron (pyramidal neurons) indicates that the postsynaptic neuron alone cannot dictate the type of synapse. We confirmed this by recording convergent innervation onto the same pyramidal neuron from different classes of interneurons in three experiments (Fig. 6A). By recording divergent connections, we also found that the same GABAergic axon can form distinct types of synapses onto different classes of target neurons (n = 3) (Fig. 6B). These data indicate that an interaction between the presynaptic and postsynaptic neurons is involved in formation of the type of synapse.

A Synaptic Homogeneity Principle

Glutamatergic synapses display differential synaptic transmission and obey a target specific rule in forming synapses (*5*, *7*), but their temporal dynamics of transmission, even onto the same class of target neuron, are highly heterogeneous (*7*). The GABAergic system is different, because interneurons form synapses with virtually identical temporal dynamics onto different targets of the same class (Fig. 6C). The connections differed in *A*, but *U*, *D*, and *F* were homogenous as could be predicted by simply normalizing each trace to the maximum amplitude—the traces overlay perfectly (Fig. 6D). In all of 22 examples of divergent connections onto two or three pyramidal neurons and involving all synapse types (F1 to F3), homogeneity was observed (Fig. 6E).

The synaptic homogeneity principle also applies across different classes of target neurons (Fig. 6F; n = 3), indicating that GABAergic interneurons are able to "select" a group of neurons to establish synapses with homogenous temporal dynamics. We term such a selected group of neurons a "GABA group." Because the same interneuron can also produce different types of synapses, each interneuron can form multiple GABA groups. All pyramidal neurons in layers II to IV are expected to be in the same GABA group together with a subset of interneurons. Other GABA groups could be composed of other classes of interneurons, spiny stellate cells, pyramidal cells in layers V and VI in the same column, and neurons in neighboring columns.

Summary

First, we found that each class of interneuron forms synapses with highly specific temporal dynamics onto a given target neuron (synapse mapping principle). This suggests that GABAergic synapses constrain the functional impact of different interneurons according to their precise timing of action potentials. Second, we found that the phenotypic nature of both presynaptic and postsynaptic neurons is involved in generating the type of synapse formed (interaction principle). This suggests that combinatorial interactions between two neurons could maximize synaptic diversity. Third, we found that interneurons form synapses with some identical properties onto neighboring target neurons (synapse homogeneity principle). This principle applies to neurons within "selected" groups. We propose that GABAergic interneurons are able to "smell out" functionally related neurons, even of different phenotypic classes, and that such "GABA groups" represent the most elementary, functionally related group of neurons identified so far in the neocortex.

References and Notes

1. S. Ramón y Cajal, *Histology Due Système Nerveux de l'Homme et des Vertébrés*, L. Azoulay, Transl. (Maloine, Paris, 1911), vol. 2.; E. White, *Cortical Circuits: Synaptic Organization of the Cerebral Cortex; Structure, Function, and Theory* (Birkhauser, Boston, 1989).
2. A. M. Thomson and J. Deuchars, *Cereb. Cortex* **7**, 510 (1997).
3. Y. Kawaguchi and Y. Kubota, *Cereb. Cortex* **7**, 47 (1997); J. DeFelipe, *Cereb. Cortex* **3**, 273 (1993); B. Cauli *et al.*, *J. Neurosci.* **17**, 3894 (1997).
4. B. W. Connors and M. J. Gutnick, *Trends Neurosci.* **13**, 99 (1990).
5. A. Reyes *et al.*, *Nature Neurosci.* **1**, 279 (1998).
6. A. Fleidervish and M. J. Gutnick, *J. Neurophysiol.* **73**, 2591 (1995).
7. H. Markram, Y. Wang, M. Tsodyks, *Proc. Natl. Acad. Sci. U.S.A.* **95**, 5323 (1998).
8. K. L. Magleby, in *Synaptic Function*, G. M. Edelman,

W. E. Gall, J. Cowman, Eds. (Wiley, New York, 1987), pp. 21–56.
9. Slice preparation, intracellular and extracellular solutions, data acquisition, model fitting, and three-dimensional (3D) reconstructions were as in (*7*). The model iterations use at least two frequencies, five responses, and the RTR. Membrane potentials were not corrected for ~9-mV junction potential.
10. Recordings were discarded because of access resistance changes, membrane instabilities, and synaptic responses below 60 μV and 1.5 pA.
11. $[Cl^-]_{out}$ = 133.5 mM and $[Cl^-]_{in}$ = 20 mM; −50.4 mV (Nernst potential); +9 mV (junction potential), expected reversal potential (V_{rev}), −41.4 mV.
12. Morphometric analysis (NeuroExplorer, MicroBrightField, Colchester, VT): Only contacts by axonal boutons within 0.37 μm were counted. Light microscopic estimates without electron microscopic confirmation can be misleading [H. Markram, J. Lübke, M. Frotscher, A. Roth, B. Sakmann, *J. Physiol.* **500**, 409 (1997)].
13. G. Tamas, E. H. Buhl, P. Somogyi, *J. Physiol.* **500**, 715 (1997).
14. Pilot studies indicated that RTR of 500 ms is optimal for separation of potentially different degrees of residual facilitation and depression.
15. Superperfusate (10 min) 0.75 mM $[Ca^{2+}]$ and 2.25 mM $[Mg^{2+}]$.
16. E. L. White, W. Weinfeld, D. L. Lev, *Somatosens. Mot. Res.* **14**, 34 (1997).
17. P. Somogyi, Z. F. Kisvarday, K. A. C. Martin, D. Whitteridge, *Neuroscience* **10**, 261 (1983).
18. Sholl analysis of the axon was used to produce a histogram of the number of axon segments found in regions progressively further away from the somata; see D. A. Sholl, *J. Anat.* **87**, 387 (1953). ASD, median in the histogram of intersections. ASL, mean interbranch length.
19. Z. F. Kisvarday, K. A. C. Martin, D. Whitteridge, P. Somogyi, *J. Comp. Neurol.* **241**, 111 (1985).
20. C. Martinotti, *Ann. Freniatr. Sci. Affini.* **1**, 314 (1889); Y. Kawaguchi and T. Shindou, *J. Neurosci.* **18**, 6963 (1998).
21. M. L. Feldman and A. Peters, *J. Comp. Neurol.* **179**, 761 (1979).
22. Possibly the same as in J. DeFelipe and A. Farien, *Brain Res.* **244**, 9 (1982).
23. M. Steriade, I. Timofeev, N. Durmuller, F. Grenier, *J. Neurophysiol.* **79**, 483 (1998).
24. Y. Kawaguchi, *J. Neurosci.* **15**, 2638 (1995).
25. J. F. Storm, *Nature* **336**, 379 (1988).
26. On the basis of methods of data sampling as well as anatomical and electrophysiological binning, the 95% confidence intervals (CIs) for the number of classes that would result if the same methods were repeated are [*11, 17*]. CI was calculated as number of classes ± 1.96 SD among 10,000 bootstrapped data sets sampled with replacement, each categorization with the identical procedure to generate a classification binning scheme [B. Efron and R. Tibshirani, *Science* **253**, 390 (1991)].
27. A Monte Carlo permutation test was applied to 10,000 shufflings of the synaptically classified cells to determine their expected distribution among 14 anatomically or physiologically defined categories. Chi-square analysis of type occurrences across categories [M. Siegel and N. J. Castellan Jr., *Nonparametric Statistics for the Behavioral Sciences* (McGraw-Hill, New York, ed. 2, 1988)] yielded $P = 3.1 \times 10^{-9}$, indicating that the probability of obtaining the observed synapse mapping randomly is negligible.
28. Model fitting of IPSCs at different voltages across V_{rev} yielded essentially identical synaptic parameters, indicating that local changes in $[Cl^-]$ do not contribute to synaptic dynamics. Model fitting of IPSPs at different membrane potentials yielded similar parameters, indicating negligible contribution of dendritic saturation and activation of nonlinearities. Near identical synaptic dynamics of divergent connections in different PCs, despite differences in IPSC/IPSP amplitudes, also indicated negligible contribution of nonlinear processes.
29. A. Gupta, Y. Wang, H. Markram, data not shown.
30. We thank E. White, Y. Yaari, I. Segev, R. Malach, and P. Goodman for comments on the manuscript. This study was supported by grants from the Office of Naval Research, the Human Frontier Science Program, the Minerva Foundation, the Israel Science Foundation, and the Nella and Leon Benziyo Center for Neurosciences. A.G. is a Minerva Fellow.

3 August 1999; accepted 11 November 1999

Rutile-Bearing Refractory Eclogites: Missing Link Between Continents and Depleted Mantle

Roberta L. Rudnick, Matthias Barth, Ingo Horn, William F. McDonough

A mass imbalance exists in Earth for Nb, Ta, and possibly Ti: continental crust and depleted mantle both have subchondritic Nb/Ta, Nb/La, and Ti/Zr, which requires the existence of an additional reservoir with superchondritic ratios, such as refractory eclogite produced by slab melting. Trace element compositions of minerals in xenolithic eclogites derived from cratonic lithospheric mantle show that rutile dominates the budget of Nb and Ta in the eclogites and imparts a superchondritic Nb/Ta, Nb/La, and Ti/Zr to the whole rocks. About 1 to 6 percent by weight of eclogite is required to solve the mass imbalance in the silicate Earth, and this reservoir must have an Nb concentration ≥ 2 parts per million, Nb/La ≥ 1.2, and Nb/Ta between 19 and 37—values that overlap those of the xenolithic eclogites. As the mass of eclogite in the continental lithosphere is significantly lower than this, much of this material may reside in the lower mantle, perhaps as deep as the core-mantle boundary.

The elements Ti, Zr, Nb, Ta, and rare earth elements (REE) are refractory and lithophile and therefore should exist in chondritic relative abundances in the silicate Earth. Continental crust and depleted mantle (DM) [mid-ocean ridge basalt (MORB) source] generally are assumed to be geochemically complementary reservoirs within the Earth. However, both reservoirs have subchondritic Nb/La (*1–4*). A similar observation is made about Nb/Ta ratios. These elements share the same valence state (+5) and have matching atomic radii (*5*), and they are thought to be geochemically inseparable. However, recent analyses (*6*) have demonstrated that Nb/Ta ratios are subchondritic in MORB and near-ridge seamounts (*7–9*), ocean island basalts (OIB) (*7, 10*), and the upper continental crust (*11, 12*). Because Nb is more incompatible than Ta in clinopyroxene during mantle melting (*13*), the DM and the source of OIB should have even lower Nb/Ta ratios. A third element ratio that also may not mass balance in Earth is Ti/Zr. The continental crust, MORB, and OIB have Ti/Zr ratios below 115, the chondritic ratio (*1*). However, because Zr is more incompatible than Ti (*13*), partial melts should have lower Ti/Zr than their source regions and the mass imbalance in this case is not clear. The DM and OIB sources could have chondritic or even superchondritic Ti/Zr [as massif peridotites do (*14*)]. Nevertheless, the subchondritic Ti/Zr in MORB and continental crust suggests that another reservoir exists that is Ti enriched relative to Zr.

The above observations require the existence of an additional reservoir that contains appreciable Nb, Ta, and Ti with superchondritic Nb/La, Nb/Ta, and Ti/Zr—features that, until now, have not been observed in common igneous and metamorphic rocks (*15*). McDonough (*1*) suggested that refractory, rutile-bearing eclogite may satisfy the mass balance requirements for Ti, Nb, and Ta in the silicate Earth. Here we show that eclogites, sampled in xenoliths from cratonic kimberlites, do indeed have the requisite trace element compositions to satisfy this mass imbalance.

Rutile (TiO_2) is a common accessory phase in metamorphic rocks and it can have

Department of Earth and Planetary Sciences, Harvard University, 20 Oxford Street, Cambridge, MA 02138, USA.